Chapter 18
Integrated Virtual Sensing Method for Real-Time Damage Detection in Mechanical Systems

Rodrigo Salazar Colunga, Nimish Pandiya, Christian Dindorf, and Frank Naets

Abstract The automotive industry seeks to improve the reliability and safety of mechanical systems while reducing maintenance costs. cro:SHMStructural Health Monitoring (SHM) provides a promising solution through real-time integrity assessments and early damage detection, helping to prevent catastrophic failures. The presented work investigates a virtual sensing approach for automotive components, combining parametric (model-based) and non-parametric (signal-based) techniques. Unlike physical sensors, which are costly and require maintenance, virtual sensors estimate difficult-to-measure quantities using data from a limited number of sensors. In this paper, the mechanical system under study is a notched aluminum beam, representative of an overhanging automotive component. Acceleration responses are acquired through vibration testing on a 3D-shaker to simulate a dynamic operational environment. A virtual sensing approach in the form of a tuned cro:KFKalman Filter (KF) is utilized to monitor the mechanical system. This work focuses on an initial assessment of the accuracy of the KF virtual sensing methodology when implemented with a generalized base excitation input in mechanical systems.

Keywords State estimation · Kalman filter · Virtual sensing · Damage detection · Structural health monitoring

Introduction

Modern vehicles operate under diverse and often unpredictable load conditions, which makes effective structural integrity monitoring essential [1]. Traditional maintenance practices based on scheduled inspections, may not adequately capture the irregular progression of wear that can lead to premature failures [2]. In this context, SHM provides real-time assessments that enable early damage detection and fatigue life prediction, supporting proactive maintenance strategies and extending component lifespan [3].

Recent literature on SHM addresses both model-based and signal-based approaches [4]. Model-based methods rely on mathematical or cro:FEFinite Element (FE) models of the structure, but their effectiveness depends on highly accurate models, often requiring complex nonlinear analyses that are computationally expensive [5]. On the other hand, signal-based methods, compare measured responses with previously acquired data to detect anomalies [6]. While being more adaptable, they depend heavily on sensor placement and availability. In many practical cases, direct measurements at critical locations are infeasible due to integration challenges or sensor limitations [7].

To address these challenges, this study presents a virtual sensing approach that combines limited sensor data with a reduced-order FE model to estimate system states. This approach is demonstrated on a notched aluminum beam tested under random base excitation on a 3D shaker. A tuned KF is employed for a full-field response estimation, enabling the

Rodrigo Salazar Colunga · Nimish Pandiya · Christian Dindorf
Robert Bosch GmbH, Center of Competence-Vibration, Robert-Bosch-Straße 2, 71707, Schwieberdingen, Germany
e-mail: rodrigo.salazarcolunga@de.bosch.com; nimish.pandiya@de.bosch.com; christian.dindorf@de.bosch.com

Rodrigo Salazar Colunga · Frank Naets
KU Leuven, Department of Mechanical Engineering, Celestijnenlaan 300, 2420 Heverlee, Belgium
e-mail: rodrigo.salazarcolunga@de.bosch.com; frank.naets@kuleuven.be

Frank Naets
Flanders Make@KU Leuven, Belgium
e-mail: frank.naets@kuleuven.be

Kristin B. Zimmerman, PhD (eds.), *Structural Health Monitoring, Metamaterials, Metastructures and Additive Manufacturing and Dynamics of Biomedical and Bioinspired Systems, 2026, Vol. 10*, Conference Proceedings
of the Society for Experimental Mechanics Series, https://doi.org/10.1007/978-8-743-81449-8_18

recovery of "difficult-to-measure" quantities. The estimated states can then be used for a variety of applications, such as predicting of stresses/strains and fatigue loads, real-time structural health monitoring or damage identification, among others [8, 9, 10, 11].

To the best of the author's knowledge, no existing formulation explicitly addresses state estimation for cro:MIMOMultiple Inputs Multiple Outputs (MIMO) cro:MDoFMultiple Degree of Freedom (MDoF) systems under applied base-excitation conditions, which motivates the approach proposed in this study.

The paper is outlined as follows: Section FE Model Validation describes the object of study, the system characterization via an cro:EMAExperimental Modal Analysis (EMA), as well as the description and validation of the FE model. Section System Modeling and Validation introduces the mathematical modeling framework for base-excited systems and its validation. Section State Estimation with Kalman Filter presents the state estimation algorithm. The results of the full-field response are presented in Section Full-field response results, and conclusions with future perspectives are stated in Section Conclusions.

FE Model Validation

System Description

The structure under study is a aluminum beam with a rectangular cross section of 5×10 mm and a length of 390 mm, cut from $AlMgSi0.5$ stocks. As shown in Figure 1, a round notch of depth 1.65 mm is machined on the long edge of the beam acting as a stress concentrator.

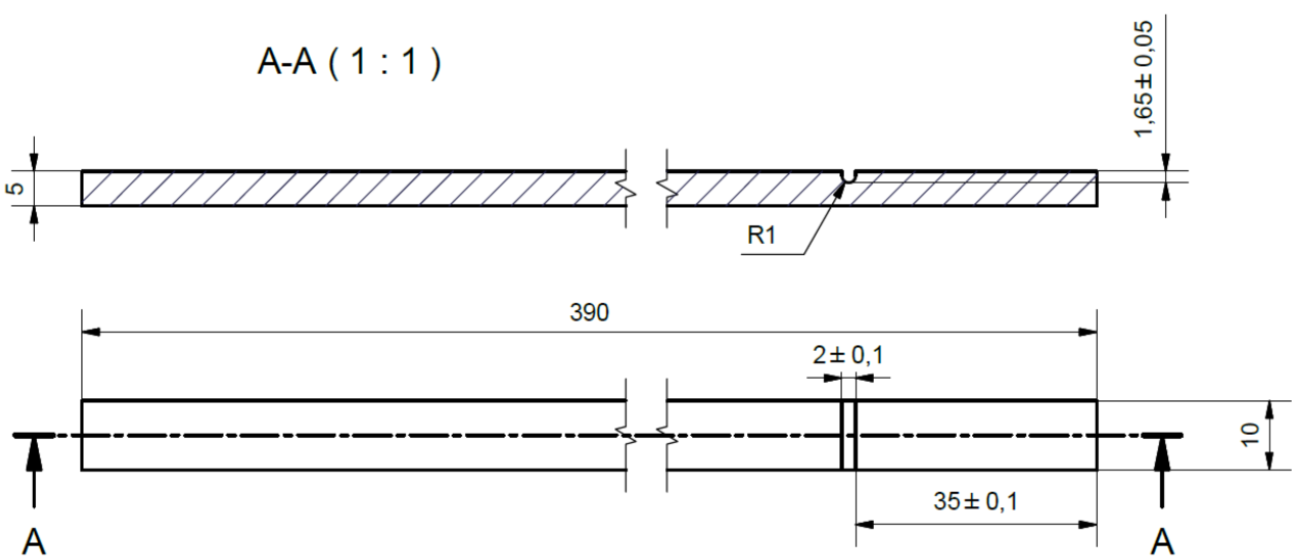

Fig. 1 Technical drawing of specimen [12]

Experimental Modal Analysis

To characterize the dynamic properties of the beam, an in-situ EMA was performed. The beam was mounted in a cantilever configuration using a fixture on the shaker table as shown in Figure 2 (left) to minimize the effect on the modelling of the boundary conditions. Five triaxial accelerometers were distributed along the beam, with Sensor $M21$ near the notch and Sensor $M25$ at the free tip as shown in Figure 2 (right) as an illustration. It can be seen on Figure 2 (left) other sensors on the fixture besides the already described, these sensors were used later for shaker control. An instrumented impact hammer was used to apply impulse excitation on the beam, and the resulting acceleration responses were recorded. This procedure enabled the identification of cro:MPModal Parameters (MP), which were later used to calibrate the numerical FE model.

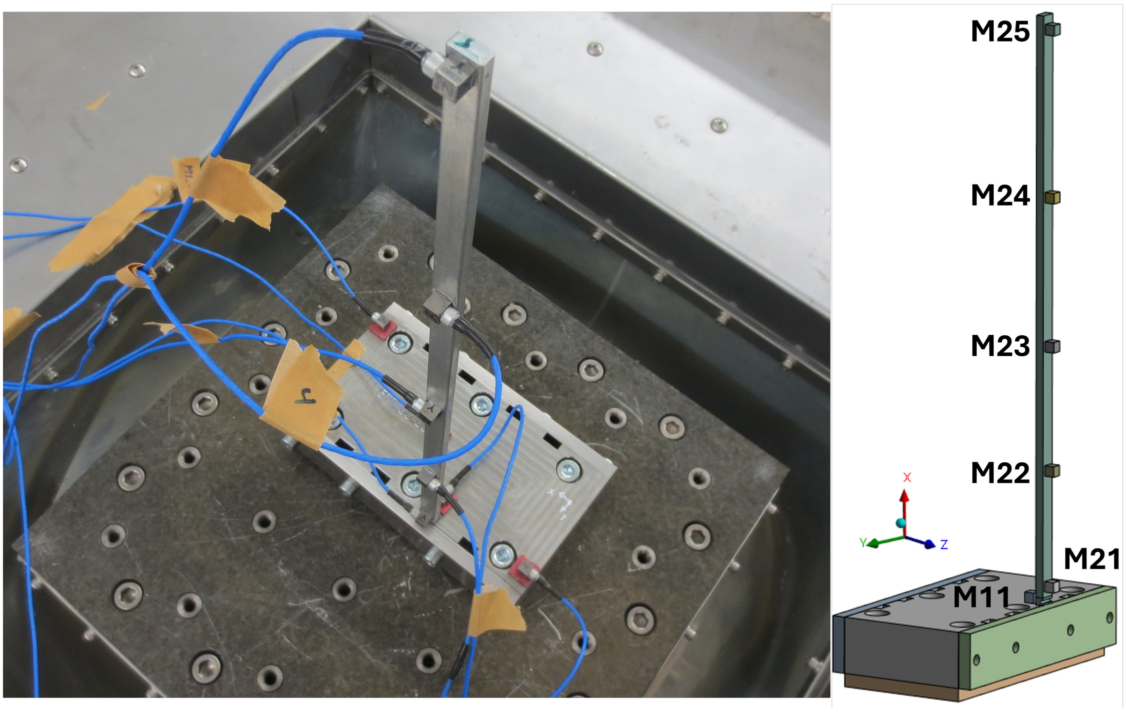

Fig. 2 Experimental (left) and FE ilustrated sensor configuration (right)

Numerical Model

A FE model of the notched beam was developed in ANSYS® Mechanical. The beam was meshed with 49980 linear HEX-SOLID185 elements, and the boundary condition at one end was defined as fully fixed to replicate the cantilever setup. Material properties were calibrated using the native parametric optimization tool in ANSYS® Workbench against the experimental modal parameters obtained from the EMA. The natural frequencies obtained experimentally and numerically are compared in Table 1. The discrepancies remain below 4% across the first seven modes, demonstrating strong agreement between the two data-sets. Furthermore, the mode shape correlation was quantified using the cro:MACModal Assurance Criterion (MAC) [13], shown in Figure 3. MAC values close to 1 confirm that the FE model reproduces the system dynamics with good accuracy. The simulated mode shape of mode 6 and 7, does not correlate with the corresponding experimental mode, but appear to be switched. No effort was made to correct this mode order because it was taken into account in the KF algorithm.

Table 1 Comparison of experimental and numerical natural frequencies.

No	FEM $f_{\text{fix-free}}$ (Hz)	Experimental $f_{\text{fix-free}}$ (Hz)	Error (%)
1	28.83	27.797	-3.58
2	55.40	56.4	+1.81
3	176.41	174.55	-1.05
4	345.36	352.47	+2.06
5	493.43	489.24	-0.85
6	963.26	958.92	-0.45
7	972.06	981.88	+1.01

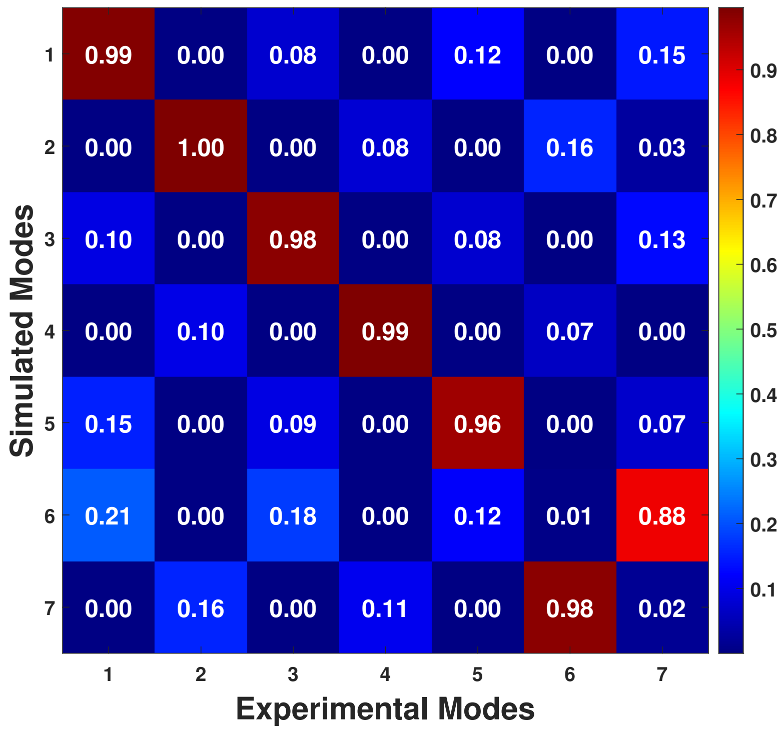

Fig. 3 Experimental and FE Modal Assurance Criterion (MAC) for the first 7 modes.

System Modeling and Validation

Equation of motion

The dynamics of a linear time-invariant mechanical system with n_{DoF} degrees of freedom can be described by the following discretized equation of motion in Eq. (1):

$$M\ddot{x}(t) + C\dot{x}(t) + Kx(t) = f(t) \tag{1}$$

where $x(t) \in \mathbb{R}^{n_{\text{DoFx1}}}$ is the displacement, and $M, C, K \in \mathbb{R}^{n_{\text{DoF}} \times n_{\text{DoF}}}$ denote the mass, damping and stiffness matrices, respectively. The external excitation is given by the force vector $f(t) \in \mathbb{R}^{n_{\text{DoF}}}$.

Eq. (1) can be reformulated for cases in which the excitation is applied as a prescribed base motion rather than a direct force input. While base-excitation formulations have been extensively studied in civil and earthquake engineering, where they are typically restricted to cro:SIMOSingle Input Multiple Outputs (SIMO) systems [14] as shown in Eq. (2):

$$M\ddot{x}(t) + C\dot{x}(t) + Kx(t) = -ML_o\ddot{x}_g(t) \tag{2}$$

where L_o is the ground input selection vector, specifying locations of the applied base excitation, typically a column vector of ones indicating that the input is applied equally to all degrees of freedom. Relative displacement of the mass with respect to the ground is represented by $x(t)$ and the imposed ground acceleration by $\ddot{x}_g(t)$.

It is worth emphasizing that the extension of this approach to MIMO MDoF mechanical system remains relatively unexplored. This motivates the present work, which develops and validates a generalized formulation suitable for mechanical structures. Such systems are typically modeled using FE models, where motion is described in terms of coupled displacements in the x, y and z directions. A generalized partition of the system can be performed on the basis of b and f nodes in Eq. (3):

$$\begin{bmatrix} M_{bb} & M_{bf} \\ M_{fb} & M_{ff} \end{bmatrix} \begin{bmatrix} \ddot{x}_b \\ \ddot{x}_f \end{bmatrix} + \begin{bmatrix} C_{bb} & C_{bf} \\ C_{fb} & C_{ff} \end{bmatrix} \begin{bmatrix} \dot{x}_b \\ \dot{x}_f \end{bmatrix} + \begin{bmatrix} K_{bb} & K_{bf} \\ K_{fb} & K_{ff} \end{bmatrix} \begin{bmatrix} x_b \\ x_f \end{bmatrix} = \begin{bmatrix} f_b(t) \\ f_f(t) \end{bmatrix} \tag{3}$$

where the subscripts b and f denote the base and free cro:DoFsDegrees of Freedom (DoFs) of a FE model, respectively. The portion of Eq. (3) corresponding to the free nodes (x_f) constitutes the unknown equation to be solved for the system response under base acceleration. The base nodes (x_b) are typically prescribed by the imposed ground input, so their values are known.

By introducing the relative displacement of the free nodes with respect to the base, defined in Eq. (4), into Eq. (3), the expression for x_f can be reformulated as shown in Eq. (5)

$$x_r(t) = x_f(t) - x_b(t) \tag{4}$$

$$M_{ff}\,\ddot{x}_r(t) + C_{ff}\,\dot{x}_r(t) + K_{ff}\,x_r(t) = -M_{be}\,\ddot{x}_b(t) \tag{5}$$

where:

$$M_{be} = M_{fb}L_{ob} + M_{ff}L_{of} \tag{6}$$

L_{ob} and L_{of} are Boolean selection matrices. They project the imposed base motion onto the corresponding DoFs of the system. This ensures consistent dimensions in the matrix products. By neglecting both damping and external base excitation, Eq. (5) reduces to Eq. (7), which is an homogeneous, undamped system.

$$M_{ff}\,\ddot{x}_r(t) + K_{ff}\,x_r(t) = 0 \tag{7}$$

assuming a harmonic solution of the form of Eq. (8)

$$x_r(t) = \phi\, e^{i\omega t} \tag{8}$$

with mode shape vector ϕ and natural frequency ω, substitution into Eq. (7) yields to

$$(K_{ff} - \omega^2 M_{ff})\,\phi = 0 \tag{9}$$

which represents the generalized eigenvalue problem of the system. Collecting all eigenvectors ϕ_j into the mode shape matrix $\Phi \in {}^{n_{DoF} \times n_{DoF}}$, and the corresponding eigenvalues ω_j into the diagonal matrix Ω^2 gives the following compact form

$$K_{ff}\,\Phi = M_{ff}\,\Phi\,\Omega^2. \tag{10}$$

Introducing the modal coordinate transformation of Eq. (11)

$$x(t) = \Phi q(t) \tag{11}$$

where $q(t) \in \mathbb{R}^{n_m}$, n_m being the number of modes; and premultiplying Eq. (5) by Φ^T yields the system in modal form as:

$$\Phi^T M_{ff} \Phi \ddot{q}(t) + \Phi^T C_{ff} \Phi \dot{q}(t) + \Phi^T K_{ff} \Phi q(t) = -\Phi^T\, M_{be}\,\ddot{x}_b(t) \tag{12}$$

Eq. (12) can be modally decoupled by exploiting the orthogonality conditions associated with a set of mass-normalized eigenvectors, $\Phi^T M \Phi = I$ and $\Phi^T K \Phi = \Omega^2$. Assuming proportional damping, we obtain $\Phi^T C \Phi = \Gamma$, where Γ is a diagonal matrix containing the terms $2\xi_j\omega_j$, and ξ_j denotes the j^{th} modal damping ratio. The resulting decoupled equations of motion from Eq. (12) in modal coordinates are given by Eq. (13):

$$\ddot{q}(t) + \Gamma \dot{q}(t) + \Omega^2 q(t) = -M_{\Phi be}\,\ddot{x}_b(t) \tag{13}$$

Continuous-time state space model

The dynamics of the beam can be expressed in first-order continuous-time state-space form by introducing the state vector $z(t)$ as shown in Eq.(14):

$$z(t) = \begin{pmatrix} x(t) \\ \dot{x}(t) \end{pmatrix} \in \mathbb{R}^{n_s},\ where \quad n_s = 2n_{\text{DoF}}, \tag{14}$$

The second-order relative displacement equation of motion Eq. (5) can then be reformulated as a first-order state equation as shown in Eq. (15):

$$\dot{z}(t) = A_c z(t) + B_c u(t) \tag{15}$$

where $u(t) \in \mathbb{R}^{n_p}$ is the input vector representing external forces, with n_p the number of independent inputs. The state dimension is $n_s = 2n_{DoF}$, where n_{DoF} denotes the number of DoFs. The matrices $A_c \in \mathbb{R}^{n_s \times n_s}$ and $B_c \in \mathbb{R}^{n_s \times n_p}$ define the system dynamics and the input mapping, respectively, and are constructed as:

$$A_c = \begin{bmatrix} 0 & I \\ -M_{ff}^{-1} K_{ff} & -M_{ff}^{-1} C_{ff} \end{bmatrix}, \qquad B_c = \begin{bmatrix} 0 \\ -M_{be}^{-1} \end{bmatrix} \tag{16}$$

In addition to the state equation, the system output is defined as:

$$y(t) = Cz(t) + Du(t) \tag{17}$$

This allows for the measurement or observation of specific system responses, such as displacements, velocities, or accelerations, at various DoFs. Here, $y(t) \in \mathbb{R}^{n_d}$ is the output vector, representing the measured quantities, where n_d is the number of measured outputs. The output matrix $C \in \mathbb{R}^{n_d \times n_s}$ and the feed-through matrix $D \in \mathbb{R}^{n_d \times n_p}$ are defined in Eq. (18).

$$C = \begin{bmatrix} I & 0 \\ 0 & I \\ -M_{ff}^{-1}K_{ff} & -M_{ff}^{-1}C_{ff} \end{bmatrix}, \qquad D = \begin{bmatrix} 0 \\ 0 \\ -M_{be}^{-1} \end{bmatrix} \tag{18}$$

The state-space representation can be formulated in the modal domain by using Eq. (13) and introducing Eq. (19) as the modal state vector

$$\tilde{z}(t) = [\, q(t)^T, \, \dot{q}(t)^T \,]^T \tag{19}$$

Following the same structure as Eqs. (15) and (17), the system can be expressed as:

$$\dot{\tilde{z}}(t) = \tilde{A}_c \tilde{z}(t) + \tilde{B}_c u(t) \tag{20}$$

$$\tilde{y}(t) = \tilde{C}\tilde{z}(t) + \tilde{D}u(t) \tag{21}$$

where $u(t)$ is equal to $\ddot{x}_b(t)$ representing the base acceleration inputs, and the tilde indicates quantities expressed in modal coordinates [15]. The state, input, measurement and output matrices in the modal domain are given by:

$$\tilde{A}_c = \begin{bmatrix} 0 & I \\ -\Omega^2 & -\Gamma \end{bmatrix}, \quad \tilde{B}_c = \begin{bmatrix} 0 \\ -M_{\phi be} \end{bmatrix}, \quad \tilde{C} = \begin{bmatrix} I & 0 \\ 0 & I \\ -\Omega^2 & -\Gamma \end{bmatrix}, \quad \tilde{D} = \begin{bmatrix} 0 \\ 0 \\ -M_{\phi be} \end{bmatrix}. \tag{22}$$

Discrete-time state space model

In this section the discrete-time formulation is introduced because it is used in the implementation of the KF, which operates naturally in discrete time. Using a sampling rate of $1/\Delta t$, the continuous-time state equation Eq. (15) can be discretized to obtain its discrete-time equivalent:

$$z_{k+1} = A_d z_k + B_d u_k \tag{23}$$

where k denotes the discrete time step. Since the output equation is an algebraic relation between the states and inputs at each time step, discretization does not affect its structure. Therefore, the output equation in discrete time is given by:

$$y_k = Cz_k + Du_k \tag{24}$$

where A_d and B_d are the discrete-time system matrices [16, 17] derived from their continuous-time counterparts, defined as:

$$A_d = e^{A_c \Delta t} \quad , \quad B_d = (A_d - I)A_c^{-1}B_c \tag{25}$$

Frequency Response Validation

The system cro:FRFFrequency Response Function (FRF) from Eq. (5), enables the understanding of the mechanical structures reaction to dynamic loading at different excitation frequencies. The FRF expresses the relationship between all inputs and all outputs of the system at certain frequencies.

$$H_{pq} = \frac{X_{r_p}(s)}{X_{b_q}(s)} = -(s^2 M_{ff} + sC_{ff} + K_{ff})^{-1} s^2 M_{be} \tag{26}$$

where s is the Laplace variable, representing complex frequency. The system response can also be expressed in modal coordinates by using the Eq. (13) leading to:

$$H_{pq} = \frac{\tilde{X}_{r_p}(s)}{X_{b_q}(s)} = -\Phi(s^2 I + s\Gamma + \Omega^2)^{-1} s^2 M_{\Phi be} \tag{27}$$

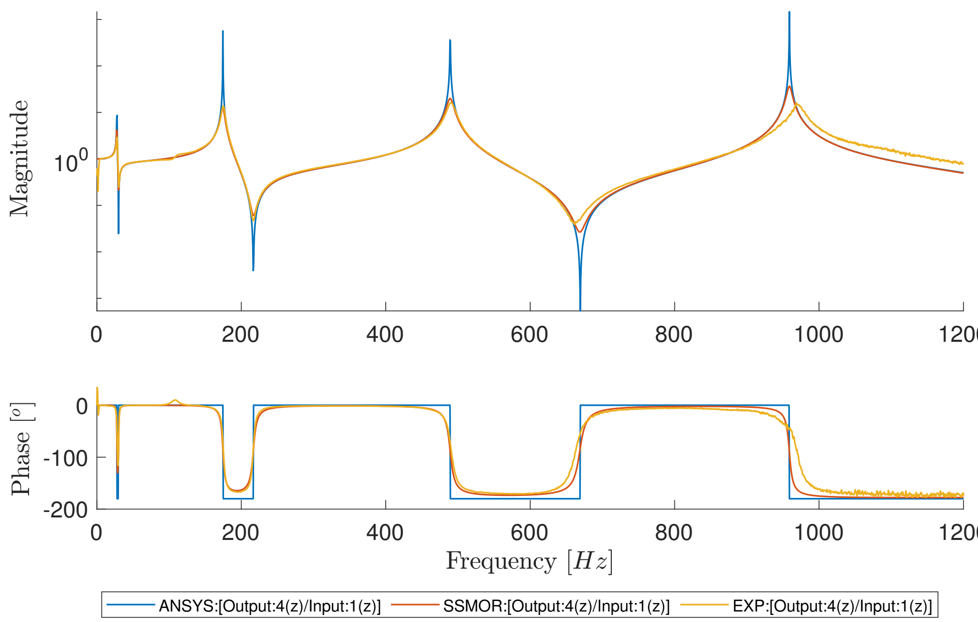

Fig. 4 Transmissibility FRF at Sensor M24 (acc/acc)

To validate the base-excitation formulation, a comparison between the FRF from the analytical reduced-order state-space model, the ANSYS ®Mechanical FE harmonic simulation, and experimental measurements was performed. Figure 4 shows the (acceleration/acceleration) transmissibility FRF from sensor $M24$. The close agreement among all three confirms the accuracy of the analytical base-excitation model.

Similar agreement is also observed at the other sensor locations, confirming the consistency of the FRF transmissibility across the system. The slight differences in peak amplitudes between the ANSYS® Mechanical FE model, and both the experimental and analytical FRFs are attributed to the fact that the ANSYS ®Mechanical simulation was performed using an undamped model.

State Estimation with Kalman Filter

The Kalman Filter (KF) is a deterministic–stochastic approach that fuses model predictions with measurement data to estimate the states of a dynamic system [18]. A key component of the KF is the cro:KGKalman Gain (KG), which enables an optimal balance between model predictions and measurement data, accounting for their respective uncertainties in an interactive way. The KF algorithm is divided into two main steps.

1. Prediction step:

$$x_{k|k-1} = A_d \hat{x}_{k-1|k-1} + B_d u_k \tag{28}$$

$$P_{k|k-1} = A_d P_{k-1|k-1} A_d^T + Q \tag{29}$$

At each step, the KF estimates the current state based on the previous state and the system model. The predicted state $x_{k|k-1}$ is projected forward in time using the system dynamics and the current input u_k, while the predicted state covariance $P_{k|k-1}$ propagates uncertainty from the previous estimate and the process noise covariance Q, which accounts for modeling errors and unmodeled disturbances [18]. The prediction is refined in the correction step.

2. Correction (or update) step:

$$S = C\, P_{k|k-1} C^T + R \tag{30}$$

$$KG = P_{k|k-1} C^T S^{-1} \tag{31}$$

$$x_{k|k} = x_{k|k-1} + KG\big(y_k - (Cx_{k|k-1} + Du_k)\big) \tag{32}$$

$$P_{k|k} = P_{k-1|k-1} - KG\,C\,P_{k-1|k-1} \tag{33}$$

where the innovation covariance S combines the predicted state covariance $P_{k|k-1}$ with the measurement noise covariance R, representing uncertainty in the sensor data. The KG determines how much the new measurement influences the state update. The state estimate $x_{k|k}$ is corrected using the measurement residual $y_k - (Cx_{k|k-1} + Du_k)$, and the state covariance $P_{k|k}$ is updated accordingly, typically reducing uncertainty. This procedure is repeated iteratively at each time step, providing an updated and more accurate state estimate over time [18].

Full-field response results

This section presents the full-field estimation using a real data-set. The data was acquired during a five minutes vibration test, where the input was a random cro:PSDPower Spectral Density (PSD) signal applied in the "Z-direction" of the beam, as shown in Figure 2 and indicated in Figure 5 by the green arrow. The acceleration on the fixture was measured by sensor $M11$, shown in Figure 2, and used as the input base acceleration on the beam. To reduce the computational effort of the large FE model, a cro:ROMReduced Order Model (ROM) of the beam was created. The ROM was built in modal coordinates, retaining 14 normal modes after applying modal truncation. For this test, only accelerometers were used. Out of the five measured responses along the beam, only accelerometer $M24$ was taken as the observation in the KF. This approach represents a "best-case" scenario in which a single measurement is used to estimate the responses at the remaining four locations, as might occur when sensor availability is limited or when other locations are inaccessible. The other accelerometer responses were estimated by the KF, and the predicted responses were compared against the measured data to evaluate the performance of the KF. The parameters for the KF implementation were:

- initial state vector set to zero,
- initial covariance P_0 set to ten,
- noise covariance matrix R defined as a diagonal matrix based on static test measurement, and
- process noise covariance Q defined under the assumption that uncertainty in uncorrelated modes is higher than in correlated ones.

Figures 6–9 show the *measured* and *estimated* acceleration responses over the first 50 seconds of the test for each accelerometer along the beam. The left panel of the figures shows the complete time history of the acceleration response, showing the complete dynamic behavior of the beam under base excitation. The right panel provides a detailed view of a segment of the response. Furthermore, the cro:NRMSENormalized Root Mean Square Error (NRMSE) between the *estimated* and *measured* acceleration time histories at accelerometers $M21$–$M25$ was calculated using Eq. (34) and the results are reported in Table 2.

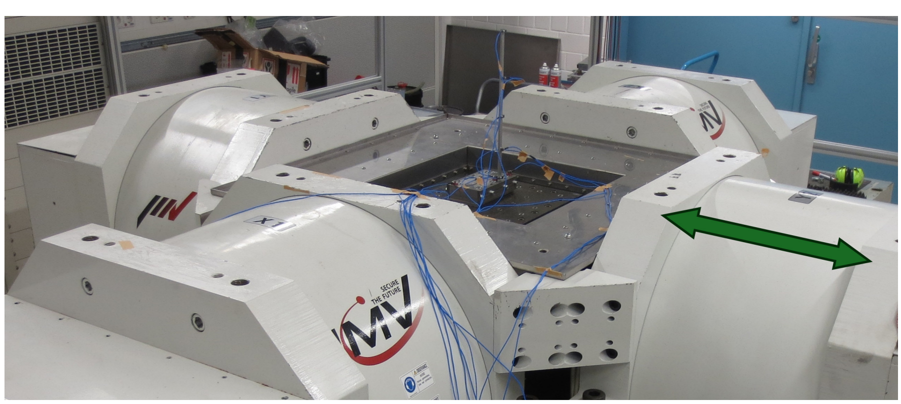

Fig. 5 Random vibration test setup on the electrodynamic 3D shaker. The green arrow indicates the excitation direction.

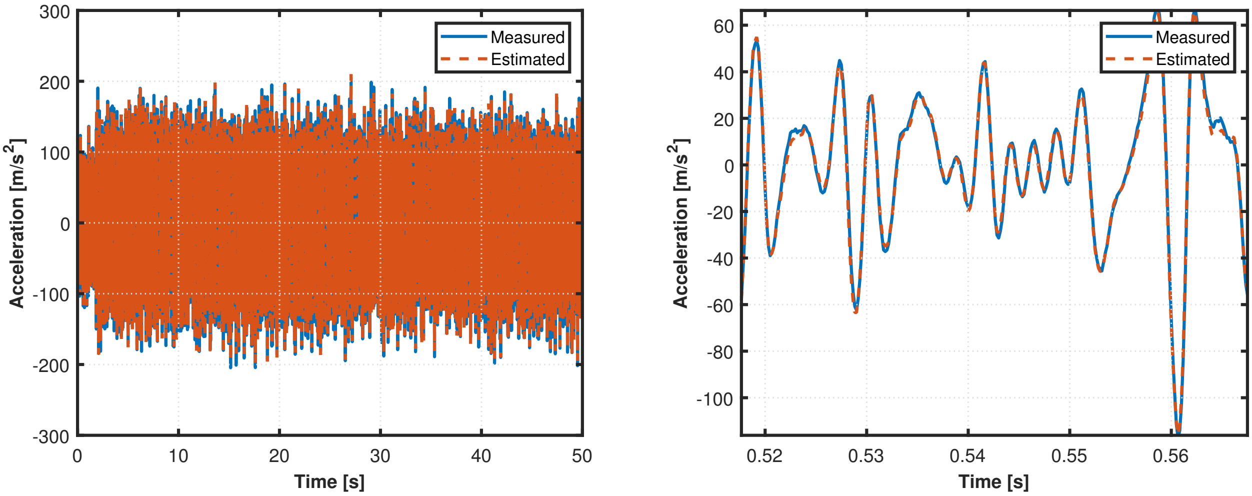

Fig. 6 Response at accelerometer M21: full time history (left) and detail (right).

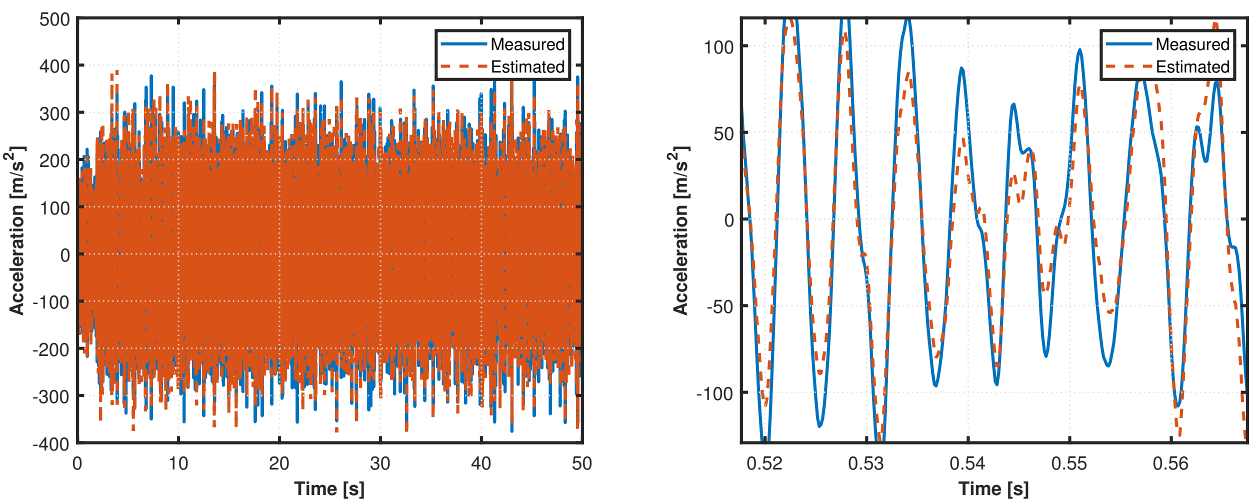

Fig. 7 Response at accelerometer M22: full time history (left) and detail (right)

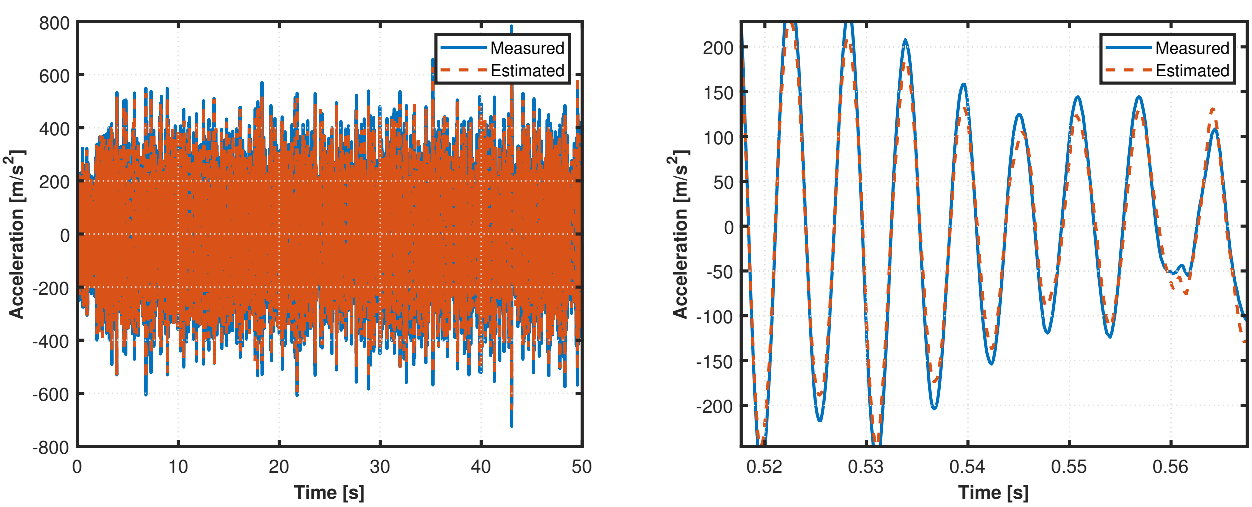

Fig. 8 Response at accelerometer M23: full time history (left) and detail (right)

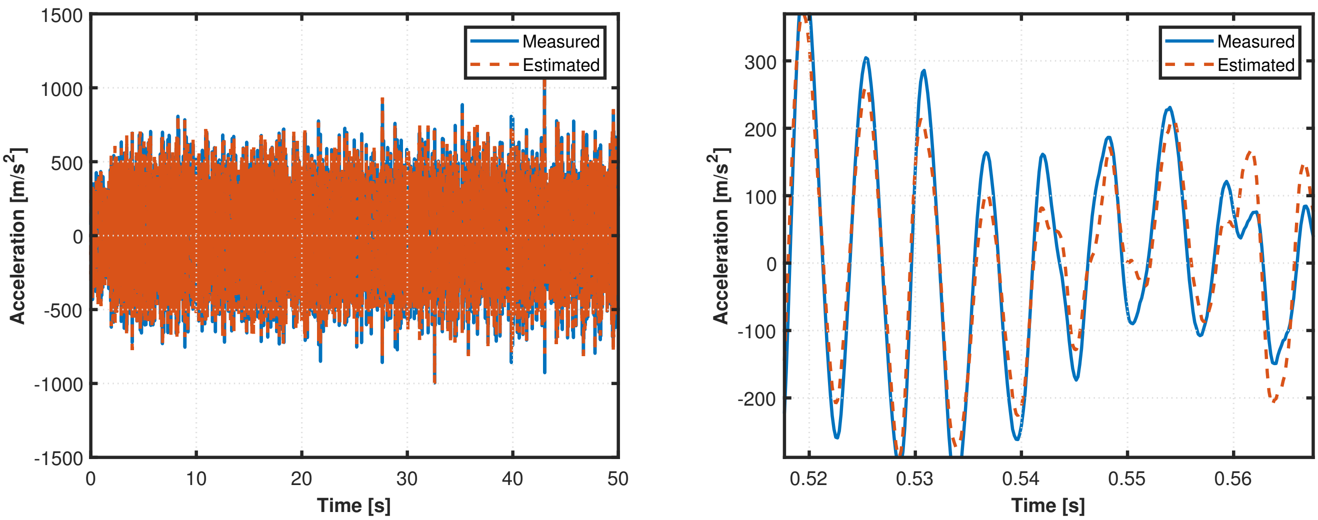

Fig. 9 Response at accelerometer M25: full time history (left) and detail (right)

Table 2 NRMSE between measured and estimated acceleration at sensors M21–M25.

Sensor	NRMSE [%]
M21	2.95
M22	10.28
M23	3.55
M24	8.74×10^{-14}
M25	4.83

$$\mathrm{NRMSE} = \frac{\sqrt{\frac{1}{N}\sum_{i=1}^{N}\left(y_i - \hat{y}_i\right)^2}}{\max(y) - \min(y)}, \tag{34}$$

where y_i and $\hat{y}_i$ denote the *measured* and *estimated* signals at time step i, respectively, and N is the number of samples. The numerator corresponds to the cro:RMSERoot Mean Square Error (RMSE), while the denominator normalizes the error with respect to a range [19]. For the calculation of the NRMSE value, the 50 seconds of data was used. The lowest NRMSE among the estimated sensors was obtained at sensor $M21$ (2.95%), which is the accelerometer closest to the notch region of the beam. Sensor $M23$ also showed a low NRMSE value of 3.55%, confirming that the estimator performs reliably at intermediate locations along the structure. Higher NRMSE values appeared at sensor $M22$ and $M25$, 10.285% and 4.831%, respectively. However, these locations are not the main analysis goal, and even at sensor $M22$, the NRMSE remains within an acceptable range. Therefore, the estimation accuracy can still be considered satisfactory across the structure. The NRMSE value between *measured* and *estimated* responses at sensor $M24$ was essentially negligible, which is expected since $M24$ was used as the observation measurement in the KF.

Conclusions

This work presented the application of virtual sensing techniques on a notched aluminum beam subjected to base excitation. The acceleration measured on the fixture was taken as the input base excitation, together with five acceleration responses measured on the beam. A KF was then employed to estimate the responses at *unmeasured* locations from a single sensor observation.

From the results presented on Table 2, it is clear that estimation accuracy varies slightly across the beam. The KF was tuned to achieve the best estimation with the smallest NRMSE value at sensor $M21$. This criteria was chosen due to the proximity of sensor $M21$ to the notch of the beam, which can be defined as a zone prone to damages in the studied structure.

Overall, these findings demonstrate that the KF can accurately reconstruct the dynamic response of a beam subjected to a base excitation using limited measurements. Although this study considered a single "best-case" scenario using only one observation, it demonstrates that high estimation accuracy can still be achieved on the other location. Future work will focus on optimal sensor placement strategies, the application of virtual sensing under multi-directional excitation to predict full-field responses of mechanical systems, and the use of this approach for real-time monitoring and structural damage detection.

Acknowledgments The authors gratefully acknowledge the European Commission for its support of the Marie-Sklodowska Curie program through the GAP_NOISE project (GA No. 101073014). Views and opinions expressed are however those of the authors only and do not necessarily reflect those of the European Union. The European Union cannot be held responsible for them. Internal Funds KU Leuven are gratefully acknowledged for their support.

References

1. Eva Katta, Kundan Maji, Satya Saha, and Sanjay Tiwari. Commercial vehicle proximal load monitoring through measuring spring deflection. Technical report, SAE Technical Paper, 2025.
2. Francesc Pozo, Diego A Tibaduiza, and Yolanda Vidal. Sensors for structural health monitoring and condition monitoring. *Sensors*, 21(5):1558, 2021.
3. Haoju Hu, Huan Luo, and Xiaoqiang Deng. Health monitoring of automotive suspensions: A lstm network approach. *Shock and Vibration*, 2021(1):11, January 2021.
4. Roberta Cumbo, Daniel De Gregoriis, Federico Danzi, Abhishek Kumar, and Frank Naets. Recursive parameter estimation for the on-line monitoring of delamination growth in composite structures. *Structural Health Monitoring*, page 20, 2024.
5. Yi Zou, Liyong Yong Tong, and Grant P. Steven. Vibration-based model-dependent damage (delamination) identification and health monitoring for composite structures — a review. *Journal of Sound and Vibration*, 230(2):357–378, 2000.
6. Christoph Kralovec and Martin Schagerl. Review of structural health monitoring methods regarding a multi-sensor approach for damage assessment of metal and composite structures. *Sensors*, 20(3):826, 2020.
7. Frank Naets, Jan Croes, and Wim Desmet. An online coupled state/input/parameter estimation approach for structural dynamics. *Computer Methods in Applied Mechanics and Engineering*, 283:1167–1188, January 2015.
8. Tulay Ercan and Costas Papadimitriou. Optimal sensor placement for reliable virtual sensing using modal expansion and information theory. *Sensors*, 21(10):3400, 2021.
9. Peng Ren and Zhi Zhou. Strain response estimation for the fatigue monitoring of an offshore truss structure. *Pacific Science Review*, 16(1):29–35, 2014.
10. Bartomeu Mora, Jon Basurko, Urko Leturiondo, and Joseba Albizuri. Strain virtual sensing applied to industrial presses for fatigue monitoring. *Sensors*, 24(11):3354, 2024.
11. Bruna Nabuco, Marius Tarpø, Ulf T Tygesen, and Rune Brincker. Fatigue stress estimation of an offshore jacket structure based on operational modal analysis. *Shock and Vibration*, 2020(1):7890247, 2020.
12. Kurthan Kersch. *3D - Vibration Testing for Automotive Components*. Phd thesis, Otto-von-Guericke-Universität Magdeburg, Germany, October 2020. Available at http://dx.doi.org/10.25673/35154.
13. David J Ewins. *Modal testing: theory, practice and application*. John Wiley & Sons, 2009.
14. Sdiq Anwar Taher, Jian Li, and Huazhen Fang. Simultaneous seismic input and state estimation with optimal sensor placement for building structures using incomplete acceleration measurements. *Mechanical Systems and Signal Processing*, 188:110047, 2023.
15. Julian Staiger. *Broad Frequency Range State, Input and Parameter Estimation for Structural Applications*. Phd thesis, KU Leuven, 03-21 2025.
16. Gene F. Franklin, J. David Powell, and Michael L. Workman. *Digital control of dynamic systems*. Addison-Wesley, Reading, Mass, 2nd ed edition, 1990.
17. Zheng Zhang and Kil To Chong. Comparison between first-order hold with zero-order hold in discretization of input-delay nonlinear systems. In *2007 International Conference on Control, Automation and Systems*, pages 2892–2896, 2007.
18. Rudolph E. Kalman. A new approach to linear filtering and prediction problems. 1960.
19. Debaditya Chakraborty and Hazem Elzarka. Performance testing of energy models: are we using the right statistical metrics? *Journal of Building Performance Simulation*, 11(4):433–448, 2017.